Markovian Models of Low and High Activity Levels of Cardiac Ryanodine Receptors

Elena Saftenku,*† Alan J. Williams,* and Rebecca Sitsapesan*

*Department of Cardiac Medicine, The National Heart & Lung Institute at Imperial College School of Medicine, London, SW3 6LY, United Kingdom; and †The Bogomoletz Institute of Physiology, Kiev, Ukraine

ABSTRACT   The modal gating behavior of single sheep cardiac sarcoplasmic reticulum (SR) Ca^{2+}-release/ryanodine receptor (RyR) channels was assessed. We find that the gating of RyR channels spontaneously shifts between high (H) and low (L) levels of activity and inactive periods where no channel openings are detected (I). Moreover, we find that there is evidence for multiple gating modes within H activity, which we term H1 and H2 mode. Our results demonstrate that the underlying mechanisms regulating gating are similar in native and purified channels. Dwell-time distributions of L activity were best fitted by three open and five closed significant exponential components whereas dwell-time distributions of H1 activity were best fitted by two to three open and four closed significant exponential components. Increases in cytosolic $[Ca^{2+}]$ cause an increase in open probability (Po) within L activity and an increase in the probability of occurrence of H activity. Open lifetime distributions within L activity were Ca^{2+} independent whereas open lifetime distributions within H activity were Ca^{2+} dependent. This study is the first attempt to estimate RyR single-channel kinetic parameters from sequences of idealized dwell-times and to develop kinetic models of RyR gating using the criterion of maximum likelihood. We propose distinct kinetic schemes for L, H1, and H2 activity that describe the major features of sheep cardiac RyR channel gating at these levels of activity.

INTRODUCTION

In cardiac cells, Ca^{2+} influx through L-type Ca^{2+}-channels triggers the opening of RyR channels thereby releasing Ca^{2+} from the sarcoplasmic reticulum (SR) causing muscle contraction. Such a mechanism of Ca^{2+}-induced Ca^{2+} release (CICR) would be expected to be a regenerative, all-or-nothing process and yet it has been shown that the release of SR Ca^{2+} and the subsequent cardiac cell contraction are very tightly controlled by the Ca^{2+} entering the cell through the L-type Ca^{2+} channel. The mechanisms underlying Ca^{2+} activation and inactivation of RyR channels are therefore the subject of intense interest as the elucidation of the mechanisms governing the regulation of RyR channel gating would help to resolve the paradox of the control of SR Ca^{2+} release.

RyR channel gating has been shown to change spontaneously during steady-state recording (Ashley and Williams, 1990; Percival et al., 1994; Zahradníková and Zahradník, 1995; Armisén et al., 1996; Copello et al., 1997). It has been proposed that the spontaneous changes in Po result from slow transitions between discrete modes of activity (Zahradníková and Zahradník, 1995, 1996; Armisén et al., 1996). Active modes of high (H) and low (L) Po levels and an inactive (I) mode were suggested. Modal gating of RyR channels has been suggested to account for heterogeneous responses of RyR channels to modulators of channel gating (Percival et al., 1994; Zahr-

adníková and Zahradník, 1995; Copello et al., 1997) and also for the phenomenon of adaptation, observed after rapid elevation of cytosolic Ca^{2+} by flash photolysis of a caged Ca^{2+} compound (Zahradníková and Zahradník, 1995, 1996; Armisén et al., 1996). It was suggested that rapid Ca^{2+} elevations cause the channel to first enter H mode and then slowly cycle between all three modes. Recently there has also been speculation that adaptation and inactivation of RyR channels can be described as manifestations of the same mechanism (Györke, 1999).

There are, however, a number of inconsistencies in relating modal gating to previously published work on the steady-state gating of RyR channels and to the phenomenon of adaptation. Modeling of the modal behavior of cardiac RyR by Zahradníková and Zahradník (1996) was based on data from steady-state recordings where the open and closed lifetimes did not change with increasing $[Ca^{2+}]$ and the slight increases in Po were brought about solely by a change in the relative areas of the three closed time constants. In addition, the characteristics of modal gating were based on data obtained at one cytosolic $[Ca^{2+}]$ (15 μM) (Zahradníková and Zahradník, 1995). Most reports of Ca^{2+} activation of the cardiac RyR, however, document larger increases in Po and changes to the closed and/or open lifetime constants (Rousseau and Meissner, 1989; Ashley and Williams, 1990; Chu et al., 1993; Sitsapesan and Williams, 1994b; Laver et al., 1995). In addition, the models of Zahradníková and Zahradník (1996) and Zahradníková et al. (1999) were based on the channel gating in two open states. In contrast, analysis of the open lifetime distribution of the Ca^{2+}-activated sheep cardiac RyR consistently indicates at least three open states (Sitsapesan and Williams, 1994b). All previously proposed models of RyR modal gating

(Zahradníková and Zahradník, 1996; Villalba-Galea et al., 1998; Zahradníková et al., 1999) in addition to other models of RyR gating (Tang and Othmer, 1994; Schiefer et al., 1995; Cheng et al., 1995; Sachs et al., 1995; Keizer and Levine, 1996; Stern et al., 1999) were chosen to reproduce the observed phenomena of adaptation or Ca^{2+}-dependent inactivation, and the information from lifetime distributions was used to adjust the rate constants. The rate constants of the models were not estimated from the sequence of dwell times nor were the hypothesized kinetic schemes chosen on the basis of statistical evaluation and ranking of the most suitable models. In this communication we present the first study to quantitatively model RyR gating using maximum likelihood estimation of rate constants from idealized data containing missed events (Qin et al., 1996). The rate constants for a number of proposed models of H1, H2, and L activity were estimated separately and hypothesized kinetic schemes were assessed statistically.

Our results demonstrate that both native and purified channels exhibit similar modes of gating. The results also show that all active modes of gating are modulated by the cytosolic $[Ca^{2+}]$. We propose different Markovian models of RyR gating for high and low levels of channel activity, selected by maximum likelihood fitting to experimentally observed dwell times at several cytosolic $[Ca^{2+}]$.

MATERIALS AND METHODS

Bilayer experiments

Preparations of SR membrane vesicles from sheep hearts, purification of RyR channels, and planar phospholipid bilayer methods were performed as described (Sitsapesan and Williams, 1994b). After incorporation of SR vesicles or proteoliposomes containing the purified RyR into a bilayer, both *cis* and *trans* chambers were perfused with a solution containing either 250 mM Cs^+ or 210 mM K^+ as described previously (Sitsapesan and Williams, 1994b).

Data acquisition and analysis

Data were recorded on digital audio tape (DAT), low-pass filtered at 2 kHz (-3 dB) with an 8-pole Bessel filter and digitized at 40 kHz using pCLAMP 6.0.3 software (Axon Instruments, Foster City, CA). Recordings of channel activity were made at -40 mV and $+40$ mV, and continuous recordings of between 30 s and 6 min in duration were used for analysis. The half-amplitude criterion was used to determine opening and closing transitions. The dead time determined by the duration of a rectangular pulse, which, when filtered, reaches 50% of its true amplitude, was 0.16 ms.

Open and closed experimental (and simulated) intervals were binned as the logarithm of their duration with 18 bins per log unit. Individual lifetimes (both experimental and simulated) were fitted to a probability density function (pdf) using the method of maximum likelihood with a correction for missed events (Colquhoun and Hawkes, 1995). Events shorter than the dead time were excluded from all distributions, and distributions were checked for artifactual components by fitting after exclusion of intervals less than twice the dead time. The number of significant exponential components in the lifetime distributions was determined with the likelihood ratio test (Rao, 1973; Horne and Lange, 1983).

The number of exponential components was increased until the improvement of the fit with the extra component was no longer significant ($p < 0.05$).

To construct the conditional open-time distributions, the contiguous closed-time ranges centred around the time constants of the components of the closed time distribution were defined. Then the open intervals occurring immediately before and immediately after closed intervals of each range were separated into groups and pdfs were fitted to conditional open-time distributions. The mean durations of the preceding open intervals and following open intervals were calculated from fitted parameters and plotted against the mean duration of the closed intervals for each specified range of closed interval duration. The dependence of the mean closed time on the duration of the adjacent open intervals was calculated in the same way, after sorting the closed intervals into groups based on the durations of adjacent open intervals (McManus et al., 1985; McManus and Magleby, 1989).

The probability of identical mode segments occurring consecutively as a result of a random association was tested by using 2×2 or 3×3 contingency tables (Nowycky et al., 1985). The observed and expected outcomes from a random distribution of consecutive segment pairs were tested by χ^2 test with $n^2 - 2n + 1°$ of freedom, where n is the number of rows or columns in the contingency table. The probability of a random distribution of consecutive segment pairs is equal to the multiple of the probability of occurrence of each kind of segment. Simulations of channel activity were carried out using CSIM (Axon Instruments). The fitting programs used in this study and programs for calculation of Po and average open durations for each segment of time, for fitting the theoretical lifetime distributions and calculation of equilibrium state occupancies, for solution of differential equations describing change of state occupancies in response to a change in $[Ca^{2+}]$ were written in Delphi3 and Borland Pascal (E. Saftenku).

Maximum likelihood analysis

Single-channel data were analyzed with maximum likelihood estimation of rate constants (Qin et al., 1996, 1997). The method employs a variable metric optimizer with analytical derivatives for rapidly maximizing the joint probability of the observed dwell-time sequence as a likelihood. This approach also applies a correction of missed events and allows multiple data sets obtained under different conditions to be fit simultaneously. We used both the Winmil program by Qin, Auerbach, and Sachs (QUB, Buffalo, NY) and our own realization of the algorithm in Borland Pascal (E. Saftenku) for the analysis of data idealized using the pCLAMP program.

A number of branched and cyclic Markovian kinetic models were examined. For cyclic models, non-independent rate constants were determined, assuming microscopic reversibility using estimated rate constants such that the product of rate constants around a cycle in the clockwise direction was equal to the product of rate constants in the anti-clockwise direction.

The Schwarz criterion (Schwarz, 1978) has been used to apply penalties for the number of free parameters and rank models. The Schwarz criterion is given by $SC = -L + (0.5F)(\ln M)$, where L is the natural logarithm of the maximum likelihood estimate, F is the number of free parameters, and M is the number of intervals. The better model has a smaller Schwarz criterion. Nested models (models derived from a general model) were compared using likelihood ratio tests (Horne and Lange, 1983; Horn and Vandenberg, 1984). For a pair of nested models, twice the difference between the maximum log(likelihood)s is distributed as χ^2. The number of degrees of freedom is equal to the difference between the number of free parameters in each model multiplied by the number of data sets. A low p value (<0.05) obtained from standard tables of χ^2 upper-tail probability indicates that the general model is statistically superior to the sub-hypothesis.

RESULTS

Fluctuating steady-state gating

At all concentrations of cytosolic free Ca^{2+} investigated (10 μM - 1 mM), fluctuations in channel activity were observed for each channel during all steady-state recordings. Fluctuations in Po with time were observed with both native and purified sheep cardiac RyR channels and at both negative and positive holding potentials. Typical examples of the spontaneous changes in gating between periods of inactivity and high, low and intermediate activity are shown in Fig. 1 for a native and a purified channel. Similar shifts in channel gating with time have been reported previously (Ashley and Williams, 1990; Percival et al., 1994; Zahradníková and Zahradník, 1995; Armisén et al., 1996; Copello et al., 1997).

Analysis of lifetime distributions

We have previously demonstrated that Ca^{2+}-dependent increases in the Po of sheep cardiac RyRs are associated with a decrease in the mean closed time (Ashley and Williams, 1990; Sitsapesan and Williams, 1994b). In contrast, no significant change in mean open time was detected although there was an obvious trend toward an increase in mean open time at concentrations of Ca^{2+} causing optimal increases in Po (Sitsapesan and Williams, 1994b). In the present study we have investigated the Ca^{2+} dependence of sheep cardiac RyR open and closed lifetimes in more detail. The simultaneous changes in Po, mean open time, and mean closed time with increasing cytosolic $[Ca^{2+}]$ are shown for native and purified sheep cardiac RyR channels in Fig. 2. In addition to the large changes in mean closed times, changes
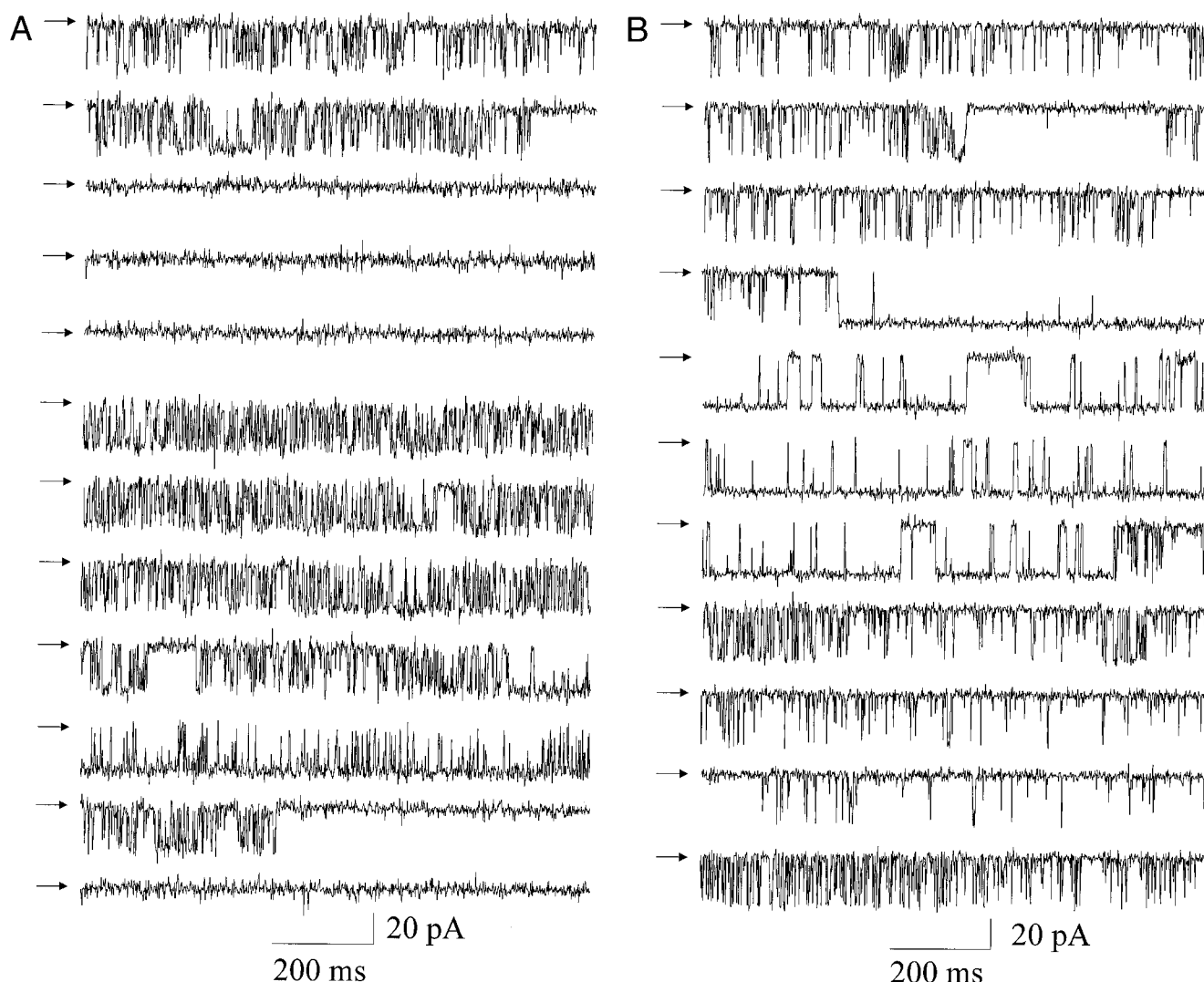

FIGURE 1 Steady-state current fluctuations through representative single sheep cardiac RyR channels incorporated into planar phospholipid bilayers at a holding potential of +40 mV. (*A* and *B*) Consecutive recordings from native and purified channels, respectively. (*A*) Channels were activated by 50 μM cytosolic Ca^{2+}; (*B*) Channels were activated by 80 μM cytosolic Ca^{2+}. The arrows indicate the closed channel levels.
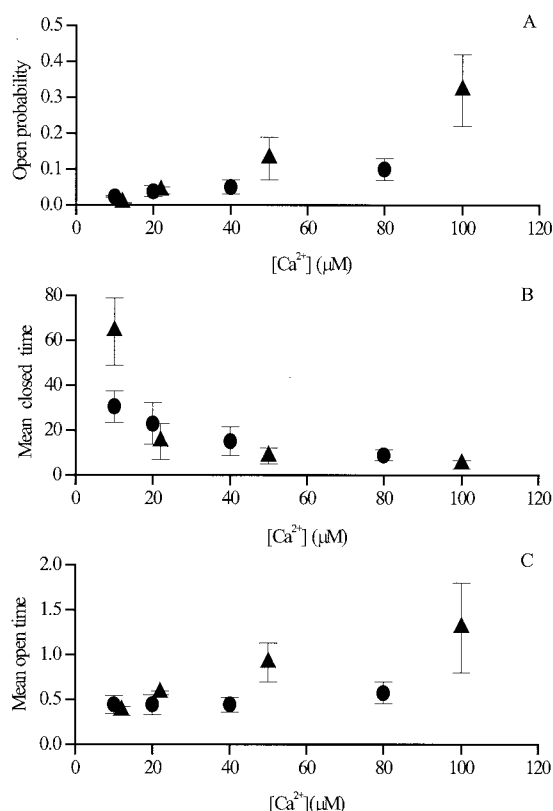
FIGURE 2   Illustration of how overall Po (*A*), mean closed time (*B*), and mean open time (*C*) change with increasing cytosolic $[Ca^{2+}]$ for both native (▲) and purified (●) channels. The mean values ± SEM for four channels are shown.

in mean open times also appeared to occur with increasing $[Ca^{2+}]$, but the increases were especially noticeable at 100 μM Ca^{2+} as can be observed in Fig. 2.

Lifetime analysis demonstrated that four or five exponential components were required to fit the closed lifetime distributions and three or four exponential components were required to fit the open lifetime distributions (not shown). This was the case for four native and four purified RyR channels. If the underlying rate constants associated with gating remain constant in time this suggests a minimum of three or four open states and four or five closed states. We found that the number of open and closed lifetime exponential components, however, shifted during steady-state gating. Moreover, as the following results demonstrate, although the number of significant exponential components describing the open and closed lifetime distributions is related to the cytosolic $[Ca^{2+}]$, the number of exponential components for a given cytosolic $[Ca^{2+}]$ varied between channels.

Characteristics of the spontaneous shifts in channel activity

To investigate the nature of the spontaneous changes in Po with time, the steady-state single-channel recordings were di-

vided into segments of 410 ms in duration. Fig. 3 illustrates how, for both purified and native channels, large changes in Po were observed. Segments of high or low Po were often grouped together over periods of several seconds, thus forming the spontaneous shifts in channel activity. Different modes of channel gating were distinguished from the distinct components of the curve that fitted the frequency distribution of Po. The minima of the fitted curve defined the threshold Po values separating the apparent modes.

Fig. 4 shows examples of the Po frequency histograms where three (*A* and *B*) or two (*C* and *D*) components were fitted. In seven of eight channels, at the higher $[Ca^{2+}]$, histograms were fitted with three components that we termed low (L), intermediate (H1), and high (H2) activity. Segments of recording where no channel openings occurred were termed inactive periods (I). For all analyzed records where different activity levels were distinguished from the Po frequency histogram, the constructed contingency tables had a probability of <0.0005 of being generated by random occurrence. Table 1 shows the expected and observed frequencies for consecutive segment pairs for the data displayed in Fig. 4. It can be seen that the probability of
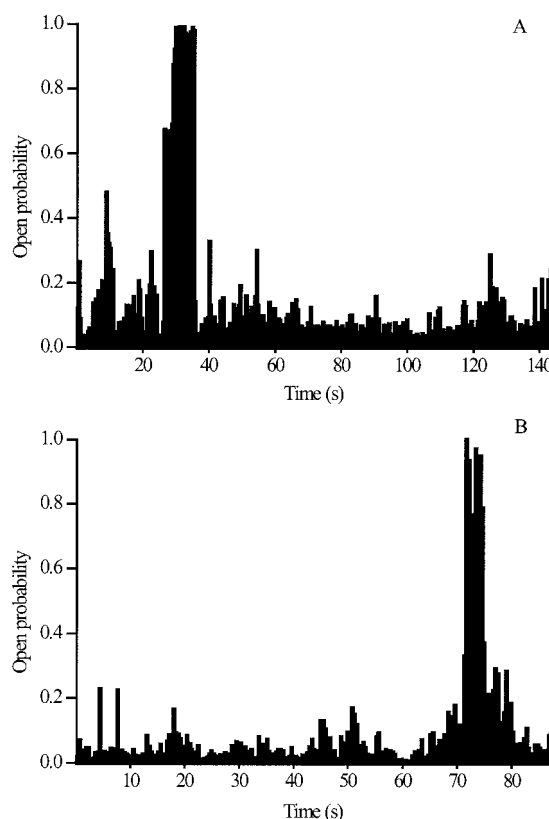

FIGURE 3   Typical examples of the shifts in Po that occur with time for a native (*A*) and a purified (*B*) channel. In both cases the holding potential was +40 mV. (*A*) The channel was activated by 50 μM cytosolic Ca^2; (*B*) The channel was activated by 80 μM cytosolic Ca^{2+}. Segment duration is 410 ms.
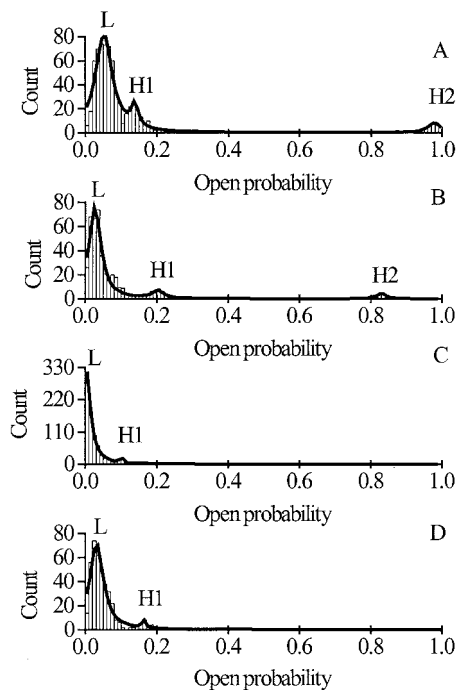
FIGURE 4 Typical examples of frequency histograms of channel Po obtained for both purified and native channels. (*A*) Data from a native channel activated by 50 μM cytosolic Ca^{2+}; (*B*) Data from a purified channel activated by 80 μM cytosolic Ca^{2+}; (*C* and *D*) Data from a native and purified channel, respectively, activated by 20 μM cytosolic Ca^{2+}. The data were best fitted by a triple (*A* and *B*) or double (*C* and *D*) Lorentz function: $y = \Sigma_i \, (2 \times A_i/\pi)\{w_i/[4(x - x_{ci})^2 + w_i^2]\}$.

that the threshold Po between L and H1 modes varied between 0.05 and 0.18 for all $[Ca^{2+}]$ whereas the threshold Po between H1 and H2 mode was in the range 0.6–0.8. The variation in Ca^{2+} sensitivity between channels made it difficult to compare H and L levels of gating activity between channels at the same $[Ca^{2+}]$. However, in all channels, both purified and native, we observed that increases in Po were associated with an increase in H activity. For example, for both purified and native channels, the probability of H1 mode occurrence was 0.008–0.1 at 10 μM Ca^{2+} but was 0.04–0.64 at $\geq$50 μM Ca^{2+}. H2 mode was detected only at high $[Ca^{2+}]$, and the probability of occurrence was less than 0.1 for the majority of purified and native channels (five of eight channels). Fig. 5 *A* demonstrates the dependence of H1 activity on $[Ca^{2+}]$.

Increasing cytosolic Ca^{2+} also increased the average Po within L mode (Fig. 5 *B*) and within H1 mode (not shown). The occurrence of I mode was much more variable as can be seen in Fig. 5 *C*. The relative occurrence of I mode varied considerably for different channels at each $[Ca^{2+}]$ (for example, the range of probability of occurrence was 0.005–0.45 ($n = 8$) at 10 μM Ca^{2+}), and no clear Ca^{2+}-dependent change in I mode occurrence for all channels was observed. In some channels there appeared to be a trend toward a decrease in I mode with increasing $[Ca^{2+}]$, with the minimum occurrence at 40–50 μM Ca^{2+}, and then a tendency for an increase in I mode occurrence again with higher $[Ca^{2+}]$. This may reflect an increasing contribution of Ca^{2+}-dependent inactivation or voltage-dependent inactivation (Sitsapesan et al., 1995; Laver and Lamb, 1998) occurring at the higher cytosolic $[Ca^{2+}]$ but requires further experimentation before any definite conclusions can be made.

We have previously described the voltage dependence of the steady-state gating of the Ca^{2+}-activated sheep cardiac RyR channel (Sitsapesan and Williams, 1994a,b) and demonstrated that Po is lower at negative holding potentials than at positive potentials. Our present results demonstrate that this could be explained both by a lower probability of the channel gating with H activity and a lower Po within L

observing a given segment type twice in succession (diagonal cells) is higher than the random prediction whereas the frequency of observing non-identical mode segments (non-diagonal cells) is lower than the random prediction.

Channels gated in L activity for 5–50 s at low $[Ca^{2+}]$ ($<$50 μM) and 0.4–10 s at high $[Ca^{2+}]$ (50–100 μM). In contrast, H1 levels of activity were observed for only 0.4–0.8 s at low $[Ca^{2+}]$ and 0.8–5 s at high $[Ca^{2+}]$. H2 activity was only observed at $[Ca^{2+}] \geq 50$ μM and occurred for durations of 2–5 s. Po frequency histograms demonstrated

TABLE 1 Frequencies per record of observed consecutive segment pairs and the random predictions (in parentheses) for the records of the channels from which frequency histograms are given in Fig. 4

	L	H1	H2		L	H1	H2
L	0.6 (0.49)	0.1 (0.18)	0 (0.03)	L	0.78 (0.68)	0.04 (0.11)	0 (0.035)
H1	0.1 (0.18)	0.15 (0.065)	0.006 (0.011)	H1	0.04 (0.11)	0.09 (0.018)	0.005 (0.006)
H2	0 (0.03)	0.006 (0.011)	0.04 (0.002)	H2	0 (0.035)	0.005 (0.006)	0.04 (0.002)

	L	H1	I		L	H1
L	0.8 (0.73)	0.04 (0.08)	0.01 (0.04)	L	0.89 (0.84)	0.029 (0.075)
H1	0.04 (0.08)	0.05 (0.009)	0 (0.005)	H1	0.029 (0.075)	0.053 (0.0066)
I	0.01 (0.04)	0.002 (0.005)	0.04 (0.003)			

L, H1, H2, and I are the segments with low, intermediate, high, and zero Po, respectively. The sequences of segments deviate strongly from the sequences expected for random distributions ($p < 0.0001$). The contingency tables for a native channel at 50 μM Ca^{2+} (upper left) and at 20 μM Ca^{2+} (lower left) as well as for a purified channel at 80 μM Ca^{2+} (upper right) and 20 μM Ca^{2+} (lower right) are shown.

mode at -40 mV in comparison with $+40$ mV. This trend can be observed in Fig. 5.

Lifetime distributions within L and H levels of channel activity

To examine the open and closed lifetime distributions for L and H activity, long sojourns of segments at low and high levels of Po were collected and analyzed separately (each segment ≥ 30 s for L activity and ≥ 10 s for H activity). Contamination between modes was evaluated by re-segmenting the records by shifting the start time of segmentation and was calculated to be less than 5%. For both native ($n = 4$) and purified ($n = 4$) channels, the open and closed lifetime distributions for H activity were best described by the sums of four open and four closed exponentials. For L activity, the open and closed lifetime distributions were best fit by the sums of three and five

exponential components, respectively. Table 2 details the lifetime analysis for L and H activity for a typical channel at various levels of cytosolic [Ca^{2+}]. These results suggest that any kinetic model that describes L activity should have at least three open and five closed states and that a different model/models should describe H activity. We cannot, however, completely exclude the possibility that an exponential component with a small area may arise as a result of inter-mode contamination.

Segments of H1 activity that we used for analysis of lifetime distributions were separated from L and H2 activity based on the determination of the threshold Po value from the Po frequency histograms and the best grouping of segments estimated from the contingency tables. More contamination between modes usually occurs when shifts between modes are more frequent and may be up to18% using this method of separating the different modes.
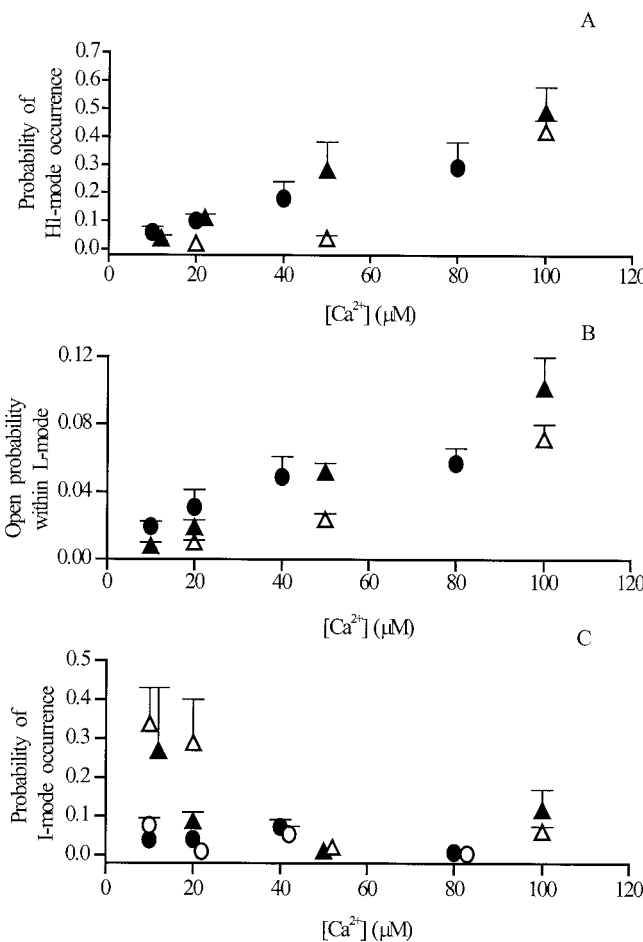
L activity level

In L activity level, increasing cytosolic [Ca^{2+}] did not change the mean open time whereas the mean closed lifetime duration was decreased (Table 2; Fig. 6). When the channels were gating with L activity, neither the time constants nor the relative areas of the open lifetime distributions were changed with increasing [Ca^{2+}]. In comparison, the closed time constants in L activity level tended to decrease with increasing [Ca^{2+}] and the distributions were shifted so

FIGURE 5 (A) Ca^{2+} dependence of the probability of occurrence of H1 mode; (B) Channel Po within L mode; (C) Probability of occurrence of I-mode. The triangles and circles are data from native and purified channels, respectively. The open and filled symbols are from recordings taken at -40 mV and $+40$ mV, respectively. The mean values $\pm$ SEM are shown.

TABLE 2 Lifetime distributions for a cardiac ryanodine receptor at low and high levels of activity

|	Calcium concentration (μM)				
	Low activity			High activity	
	10	20	50	50	100
Open time (ms)	0.22	0.2	0.22	0.28	0.28
	0.57	0.67	0.65	0.96	1.05
	3.1	3.2	3.03	4.44	2.32
				31.36	10
Relative area	0.64	0.65	0.66	0.27	0.16
	0.35	0.34	0.33	0.56	0.54
	0.008	0.01	0.006	0.11	0.28
				0.053	0.012
Mean open time (ms)	0.37	0.39	0.38	2.77	1.38
Closed time (ms)	0.15	0.18	0.29	0.35	0.34
	1.29	1.9	1.29	1.49	1.07
	7.98	10.45	6.85	7.14	2.62
	58.9	31.79	18.2	32.26	22.4
	207.6	112.61	85.16		
Relative area	0.013	0.04	0.015	0.17	0.22
	0.12	0.12	0.085	0.39	0.46
	0.25	0.34	0.55	0.42	0.32
	0.45	0.4	0.34	0.023	0.0022
	0.17	0.1	0.007		
Mean closed time (ms)	63.9	27.8	10.67	4.4	1.46
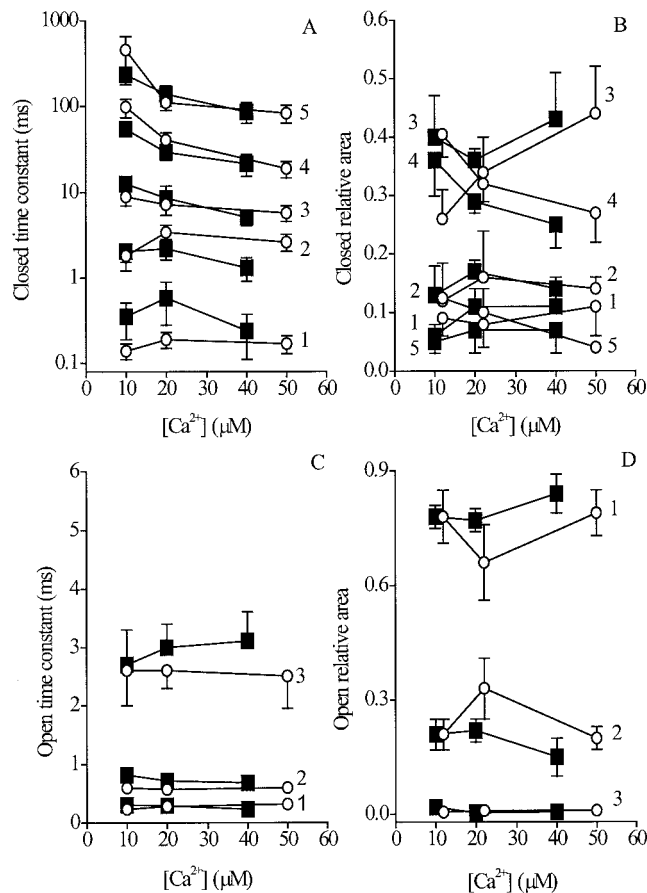
FIGURE 6 Ca^{2+} dependence of the exponential components describing the dwell-time distributions for L mode channel gating. (*A* and *B*) The five exponential components and relative areas, respectively, describing the closed lifetime distributions; (*C* and *D*) The three exponential components and relative areas, respectively, describing the open lifetime distributions. The mean values $\pm$ SEM of four experiments are shown for both native (○) and purified (■) channels.

FIGURE 7 Ca^{2+} dependence of the exponential components describing the dwell-time distributions for H1 mode channel gating. (*A* and *B*) The four exponential components and relative areas, respectively, describing the closed lifetime distributions; (*C* and *D*) The three exponential components and relative areas, respectively, describing the open lifetime distributions. The mean values $\pm$ SEM of four experiments are shown for both native (○) and purified (■) channels.

that fewer long closings and more frequent shorter closings were observed.

H activity level

Transition from L to H activity caused a general shift in the open lifetimes toward longer durations and the closed lifetimes toward shorter durations (Figs. 7 and 8). Table 2 demonstrates that the major changes in the open lifetime distributions were in the occurrence of the longest open lifetime component and a shift in the distribution of the events such that fewer events occurred with the shortest open lifetime constant. We had a low number of events in H2 mode, and therefore the analysis of H2 mode dwell times could not be performed as accurately as that of H1 mode. In H1 mode, two or three significant exponential components of the open lifetime distributions and four components of the closed lifetime distributions
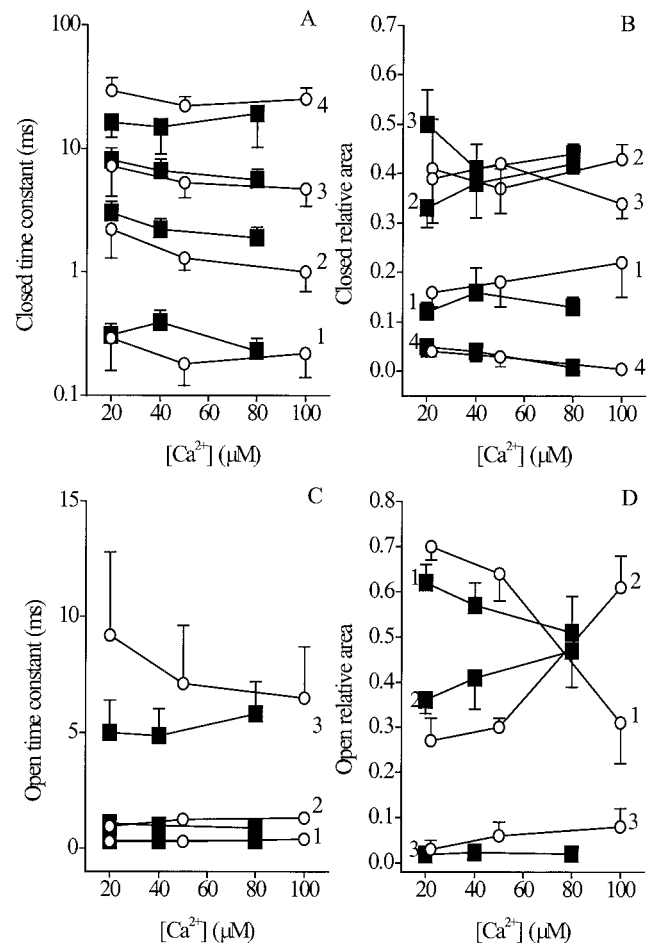
were detected. In general, open lifetime durations were longer, and more frequent longer openings were observed in H1 mode than in L mode for both native and purified channels. The mean open time for H2 activity was 26 ± 6 ms at 50 μM Ca^{2+} and 6 ± 1.2 ms at 100 μM Ca^{2+}, and the mean closed time was 0.8 ± 0.10 ms and 0.6 ± 0.10 ms at 50 μM and 100 μM Ca^{2+}, respectively. Analysis of H2 activity indicated the presence of two open exponential components with Ca^{2+}-dependent time constants of 2–8 ms and 10–40 ms and two closed exponential components with time constants of 0.3–0.5 and 4–6 ms. When all H activity was analyzed, we also observed that the two longest time constants from the open lifetime distribution became shorter and mean open and closed lifetimes were decreased when Ca^{2+} was increased from 50 to 100 μM (see Table 2). In H1 mode, the time constants of closed lifetime distributions were
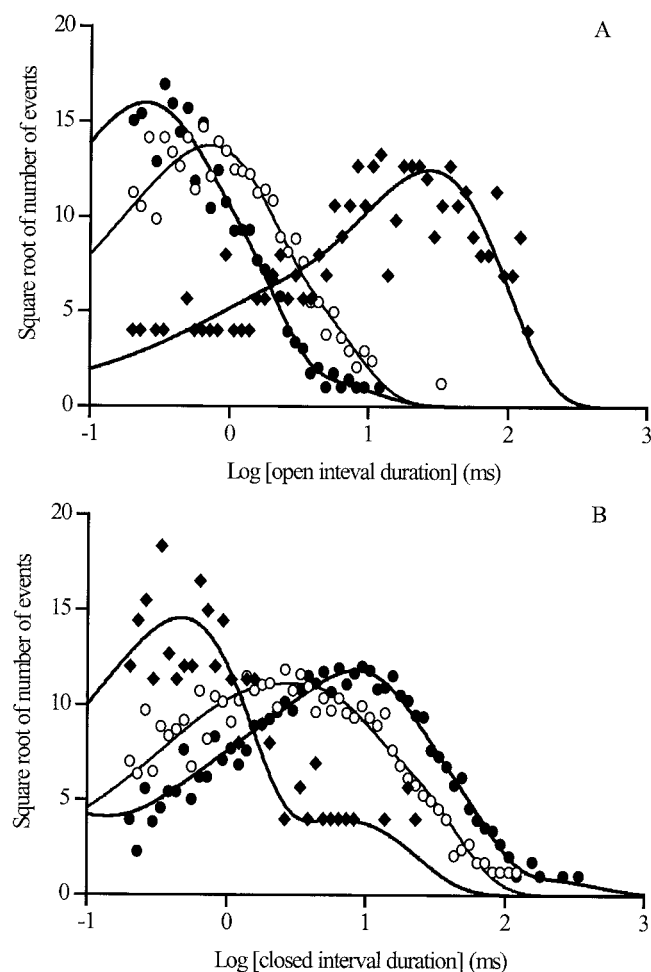
FIGURE 8 Distributions of open and closed interval durations during periods of L (●), H1 (○), and H2 (◆) channel gating activity. (A) Open lifetime distributions; (B) Closed lifetime distributions. Lifetimes from a native channel activated by 50 μM cytosolic Ca^{2+} are shown. A total of 7000 events for L activity, 5000 events for H1 activity, and 500 events for H2 activity were binned, respectively, in open and closed lifetime histograms. The numbers of binned events for each distribution was normalized to 7000 events for ease of comparison. The solid lines show the fits obtained to simulated data. The rate constants for the simulation of L activity are given in Table 4 (channel 4), and the rate constants for simulation of H1 and H2 activity are given in Results.

Ca^{2+} dependent, and open lifetime distributions were shifted so that more long openings were observed at higher $[Ca^{2+}]$ (Fig. 7).

Correlations between durations of adjacent open and closed events

To obtain information about the connections between open and closed states, the relationships between the durations of adjacent open and closed events were investigated (Colquhoun and Hawkes, 1995). The mean durations of all open events adjacent to (immediately preced-

ing and immediately following) the closed intervals in each specified range were determined and plotted against the mean of the closed interval in each specified range. Fig. 9 illustrates the relationships for adjacent open and closed intervals for typical native and purified channels, respectively. The ratios of the mean open durations immediately before and after adjacent closed intervals were close to 1 for all analyzed records of purified and native channels ($n = 8$) (see Fig. 9, A and D) as were the ratios of the mean closed durations immediately before and after adjacent open intervals (data not shown). These observations indicate the thermodynamic equilibrium of RyR channel gating. The results of analysis of the correlations between adjacent openings and closings indicate that, for both native and purified channels, in general, short openings tend to be adjacent to long closings and long openings tend to be adjacent to short closings (see Fig. 9). Similar observations were reported for the Ca^{2+}-activated K^+ channel (McManus and Magleby, 1989; McManus et al., 1985) and for NMDA-type glutamate receptors (Gibb and Colquhoun, 1992). Such a relationship can be generated by a discrete Markov model if there are two or more transition pathways between the open and closed states and if the lifetimes of the open states are, in general, inversely related to the lifetimes of the closed states to which they make direct transitions. In one native and one purified channel, however, pairs of long openings and long closings were observed. Both the open and the closed events were approximately 7 s in duration. These transitions were observed at all $[Ca^{2+}]$ and at holding potentials of both $+40$ mV and -40 mV.

The range of mean open times for the conditional distributions of open intervals together with the range of mean closed times for the conditional distributions of closed intervals were found to change significantly from one recording to another depending on the relative occurrence of H activity in the recording. When only L activity and only H1 activity were analyzed for correlations between adjacent open and closed events we again found that for both levels of activity, long closings tended to be adjacent to short openings and short closings tended to be adjacent to long openings (Fig. 9, B and C). However, the relationship was much more evident for H1 activity than for L activity, presumably because most of the longer openings do not occur at low levels of activity.

Derivation of gating schemes

Gating schemes were derived using data collected and analyzed separately for channels gating in L, H1, or H2 activity for a range of cytosolic $[Ca^{2+}]$. Hill coefficients for Ca^{2+} activation varied from channel to channel (range 1.4–5) but were always greater than 1. Such variability in Hill coefficients has been previously reported for RyR chan-
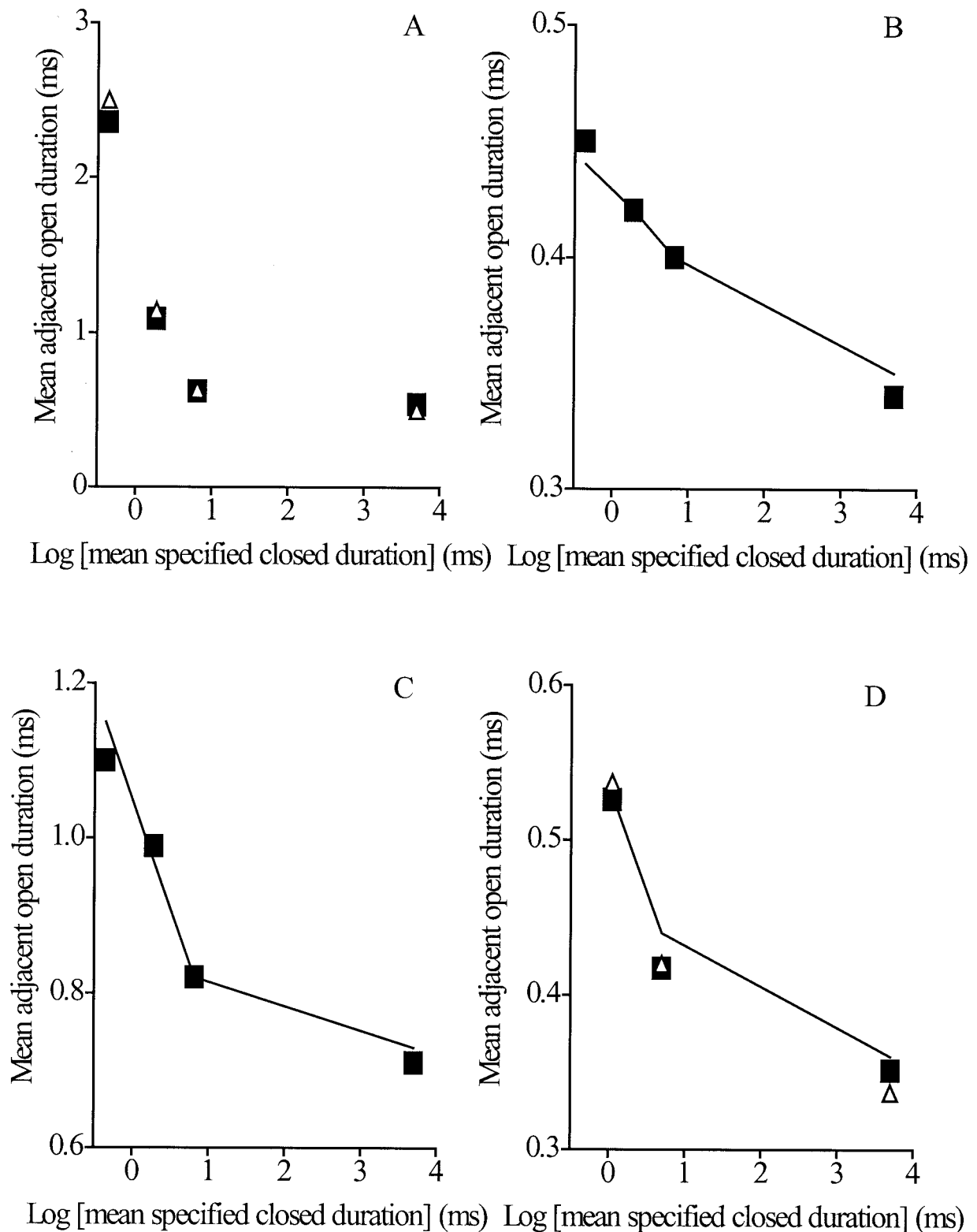
FIGURE 9   The relationship between the mean durations of adjacent open and closed intervals. The mean durations of open intervals adjacent to the closed intervals in each specified range are plotted against the mean durations of the closed intervals in each specified range. Mean durations of open intervals following the closed intervals (■) and mean durations of open intervals preceding the closed intervals (△) are shown. The relationship for the simulated data is shown by the lines. The relationship for the whole of the recording (A), only for L activity (B), and only for H1 activity (C) for a typical native RyR activated by 50 μM cytosolic Ca^{2+} is shown. The rate constants for simulation of L activity are given in Table 4 (channel 4), and the rate constants for simulation of H1 activity are given in Results. (D) Relationship between the mean durations of adjacent open and closed intervals for a purified RyR activated by 40 μM cytosolic Ca^{2+}. The data for a channel exhibiting predominantly L activity at this $[Ca^{2+}]$ are shown. The rate constants given in Table 4 (channel 1) were used for simulation.

nels (Sitsapesan and Williams, 1994b; Copello et al., 1997), and this feature of RyR channel gating prevents us assigning a definitive number of Ca^{2+} binding steps either in L, H1, or H2 levels of channel activity.

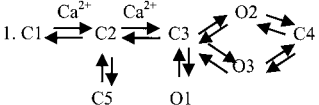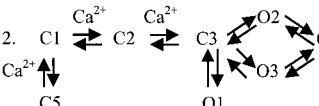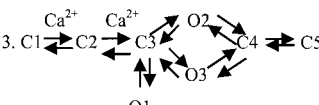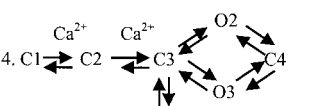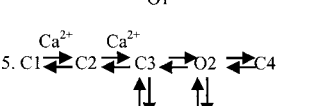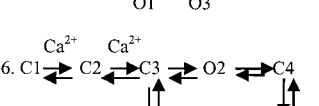## Gating schemes for L levels of channel activity

Assuming four or five closed states and two or three open states, a variety of kinetic schemes were constructed and the rate constants analyzed with maximum likelihood estimation using an algorithm described by Qin et al. (1996, 1997). When the data sets were simultaneously fitted with several $[Ca^{2+}]$, convergence of a variable metric optimizer utilized by this algorithm was not obtained when only two open states were assumed and was obtained for only three models when four closed states were assumed (Table 3; schemes 4–6). Convergence was also obtained after addition of the fifth closed state connected with states C1, C2, or C4. Table 3 presents the ranking of the various schemes based on the Schwarz criterion, which applies a penalty for increased numbers of free parameters. Convergence to these schemes occurred despite differences in some of the rate constants, and surprisingly, the same ranking of the schemes occurred with all channels analyzed ($n = 8$). Scheme 1 was always ranked above the others.

Scheme 4 is a nested sub-hypothesis of schemes 1–3 and can be compared with them statistically. Likelihood ratios showed that scheme 4 is distinguishable from schemes 1–3 ($p < 0.0001$; 6° of freedom). The results of model comparison indicate that the additional long closed state (C5) does make schemes 1–3 statistically better models.

The rate constants estimated for scheme 1, together with their standard deviations, for four separate channels are given in Table 4. Sets of data obtained at holding potentials of ± 40 mV were analyzed separately. The data sets included 30,000–60,000 events and were fitted simultaneously for two (channel 3), three (channels 1 and 4), or four (channel 2) $[Ca^{2+}]$. The sets of data at -40 mV were analyzed separately. After estimating the kinetic parameters, scheme 1 was simulated, at several $[Ca^{2+}]$, using the estimated parameters with the noise, conductance, and filter frequency of the experimental data using the program CSIM (Axon Instruments). The data were idealized with FETCHAN (pCLAMP 6), and lifetime distributions were analyzed. Average Po values for the simulated data coincided or were very close to the values obtained from the analysis of experimental distributions. For example, for channel 1 of Table 4, the Po for simulated activity was 0.024, 0.053, and 0.098 at 10, 20, and 40 μM Ca^{2+}, respectively, compared with 0.024, 0.053, and 0.1 for the experimental data. Mean closed times were 26.27, 11.89, and 5.38 ms for simulated activity at 10, 20, and 40 μM Ca^{2+}, respectively, compared with 27.00, 12.67, and 5.63 ms for the experimental data. Mean open times were 0.45 ms for all three $[Ca^{2+}]$ for both simulated and experimental data. Fig. 10, *A–D*, compares the fits to experimental open and closed lifetime distributions at 20 and 40 μM Ca^{2+} with that of the model predictions. The dependence of Po with time (with segment duration 410 ms) and the relationship between the mean durations of adjacent open and closed intervals (Figs. 9, *B* and *D*) were also very close to experimental values.

Gating schemes for H levels of channel activity

Examination of the H1 activity gating of the channel is more difficult than L activity because the probability of H1 activity occurrence is very low at $[Ca^{2+}] < 50$ μM. There is, therefore, sufficient data for analysis of H1 activity gating at only two different cytosolic $[Ca^{2+}]$. This poses problems in determining the number of Ca^{2+}-binding sites involved in H1 activity gating and in resolving which transitions are Ca^{2+} dependent. The probability of occurrence of H2 mode was low even at these two $[Ca^{2+}]$. It was also difficult to split H1 and H2 modes due to their short cross-contamination, which we observed when the length of segments was decreased. We therefore thoroughly checked the data cho-

TABLE 3 Kinetic models of the gating of cardiac ryanodine receptors at low levels of activity

Scheme	Schwarz criterion	Number of parameters
1.	1	15
2.	2	15
3.	3	15
4.	4	13
5.	5	12
6.	6	12

TABLE 4 Estimated rate constants for Scheme 1

Channel holding potential	1	2		3	4	
	+40 mV	+40 mV	−40 mV	+40 mV	+40 mV	−40 mV
C1C2 (μM^{-1} s^{-1})	2.5 ± 0.21	1.7 ± 0.28	0.83 ± 0.12	0.42 ± 0.049	1.3 ± 0.092	0.71 ± 0.041
C2C1 (s^{-1})	13.3 ± 1.6	11 ± 1.5	11 ± 1.8	9.2 ± 1.5	9.1 ± 1.8	28 ± 5.7
C2C3 (μM^{-1} s^{-1})	68 ± 8	20 ± 2.7	38 ± 7.8	16 ± 3.1	33 ± 3.2	4 ± 0.022
C3C2 (s^{-1})	8000 ± 1100	300 ± 48	1000 ± 210	1400 ± 270	5200 ± 980	7300 ± 1700
C3O2 (s^{-1})	17 ± 3.2	2 ± 0.26	3.8 ± 0.57	13 ± 2.7	43 ± 10	68 ± 16
O2C3 (s^{-1})	92 ± 9.9	25 ± 2.7	340 ± 40	310 ± 35	90 ± 10	82 ± 11
O2C4 (s^{-1})	1900 ± 130	2600 ± 240	1570 ± 190	2600 ± 230	1700 ± 210	1600 ± 150
C4O2 (s^{-1})	520 ± 35	290 ± 26	480 ± 60	440 ± 40	372 ± 27	390 ± 34
C3O3 (s^{-1})	14 ± 1.9	0.82 ± 0.12	2 ± 0.29	4.3 ± 0.82	15 ± 2.8	15 ± 3.2
O3C3 (s^{-1})	138 ± 16	23 ± 3.9	290 ± 35	120 ± 18	74 ± 20	25 ± 3.8
O3C4 (s^{-1})	300 ± 28	270 ± 27	210 ± 38	240 ± 26	280 ± 26	220 ± 24
C4O3 (s^{-1})	46 ± 5.8	10 ± 1.1	44 ± 9.6	33 ± 4.6	53 ± 6.8	74 ± 11
C3O1 (s^{-1})	1100 ± 53	120 ± 6.1	147 ± 7.2	260 ± 70	660 ± 120	2100 ± 140
O1C3 (s^{-1})	3400 ± 54	3300 ± 44	4200 ± 67	5010 ± 120	2700 ± 47	6500 ± 210
C2C5 (s^{-1})	0.13 ± 0.028	4.2 ± 0.58	4.2 ± 0.6	1.1 ± 0.26	0.58 ± 0.1	0.63 ± 0.11
C5C2 (s^{-1})	3.6 ± 0.49	5.7 ± 0.69	5.6 ± 0.68	2.7 ± 0.38	2.4 ± 0.31	1.8 ± 0.3

sen for analysis so that the contamination from the other modes did not exceed 3%.
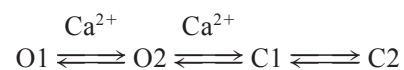
After comparison of different models with two to three open and three to four closed states, we obtained the best description of the experimental data in H1 mode with the following model:

$$
\begin{array}{ccc}
& \text{Ca}^{2+} & \text{Ca}^{2+} \\
\text{C1} \rightleftharpoons & \text{C2} \rightleftharpoons & \text{C3} \\
& \updownarrow \;\text{Ca}^{2+} & \updownarrow \;\text{Ca}^{2+} \\
& \text{O1} & \text{O2} \rightleftharpoons \text{C4}
\end{array}
$$
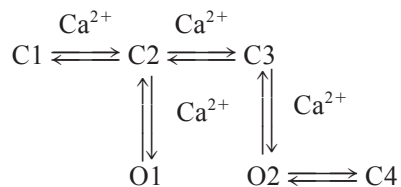
The best fit of the model to the experimental data was found when four Ca^{2+}-binding sites were assumed. Removal of any of the Ca^{2+}-binding transition led to significantly lower likelihood values or prevented the maximum likelihood algorithm from converging. The Ca^{2+}-dependent rate constants for a native and purified (in parentheses) channel were the following (μM^{-1} s^{-1}): C1C2, 3.26 (2.11); C2O1, 7.86 (11.7); C2C3, 0.66 (3.92); and C3O2, 7.77 (25.7). The Ca^{2+}-independent rate constants (s^{-1}) were: C2C1, 116 (57.4); O1C2, 1480 (1500); C3C2, 163 (263); O2C3, 330 (521); O2C4, 298 (123); and C4O2, 2390 (1240). This model of gating in H1 mode was then simulated (as for scheme 1 in L mode). Lifetime distributions and the relationships between the mean durations of adjacent open and closed intervals simulated from the model fit the experimental data well. For example, for a native channel in H1 mode, the Po for the simulated data and experimental data were both 0.16 at 50 μM Ca^{2+} and 0.45 at 100 μM Ca^{2+}. Mean closed times for simulated and experimental data were 5.01 and 4.97 ms, respectively, at 50 μM Ca^{2+} and 1.62 and 1.57

ms, respectively, at 100 μM Ca^{2+}. Mean open times for simulated and experimental data were 0.92 and 0.91 ms, respectively, at 50 μM Ca^{2+} and 1.3 and 1.28 ms, respectively, at 100 μM Ca^{2+}. A comparison of the fits to the experimental open and closed lifetime distributions at 50 and 100 μM Ca^{2+} with that of the model predictions can be found in Fig. 8 and in Fig. 10, E and F. The mean durations of the distributions of open intervals adjacent to specified closings at 100 μM Ca^{2+} were 1.42, 1.25, and 1.03 ms for simulated data and 1.47, 1.25, and 1.04 ms for experimental values.

The following scheme provided the best description of the experimental data in H2 mode and was a good fit to our experimental distributions:

$$
\begin{array}{ccc}
\text{Ca}^{2+} & \text{Ca}^{2+} & \\
\text{O1} \rightleftharpoons \text{O2} \rightleftharpoons \text{C1} \rightleftharpoons \text{C2}
\end{array}
$$

The Ca^{2+}-dependent rate constants (in μM^{-1} s^{-1}) for a native and purified (in parentheses) channels were as follows: O1O$_2$, 2.41 (1.66); O2C1, 2.62 (6.8). The Ca^{2+}-independent rate constants (s^{-1}) were as follows: O2O1, 85.1 (71.8); C1O$_2$, 2277 (1459); C1C2, 60.8 (58.4); and C2C1, 198 (201). It is important to note that the unavoidable use of the low number of events in our H2 mode data sets (2000–4000) and the simultaneous fit at only two [Ca^{2+}] essentially limits the possibility of finding the most likely scheme for this type of activity and for extracting the most accurate rate constants.

The complete model for cardiac RyR channel gating has to be described by kinetic schemes for L, H1, and H2 levels of activity that are connected by slow transitions. In addition, the transition from L to H1 activity appears to be Ca^{2+} dependent because the duration of channel sojourns in L
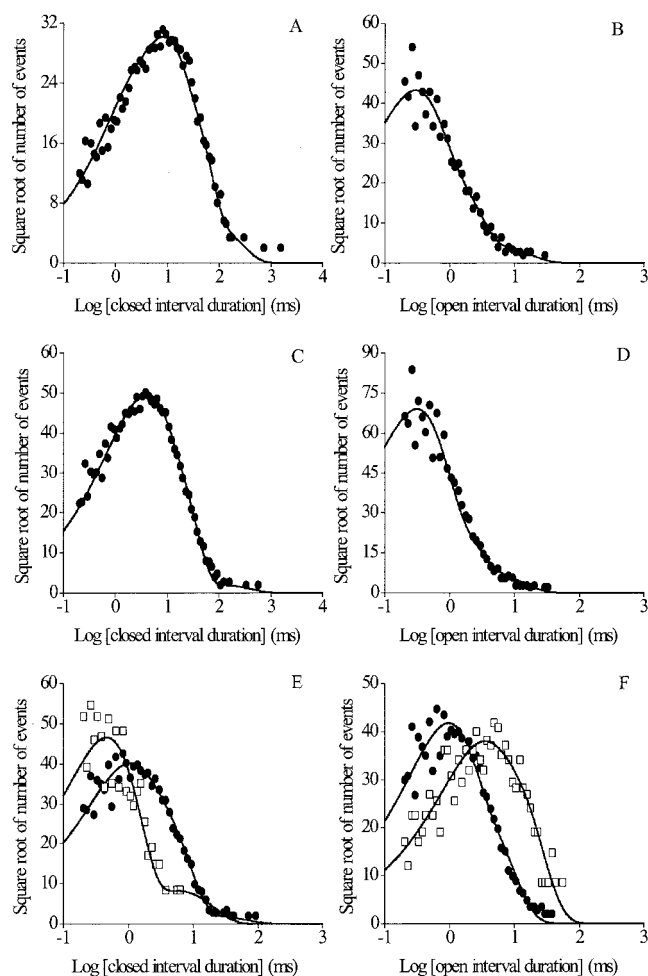
FIGURE 10   Representative examples of closed (*left*) and open (*right*) lifetime distributions from a native and purified channel illustrating both high and low activity. Data obtained from a purified channel during L activity at 20 μM Ca^{2+} (*A* and *B*) and 40 μM Ca^{2+} (*C* and *D*) are shown. Data from a native channel during H1 activity (●) and H2 activity (□) at 100 μM Ca^{2+} (*E* and *F*) are shown. The number of binned events in the distributions was 12,500 at 20 μM Ca^{2+}, 20,000 at 40 μM Ca^{2+}, 17,500 for H1 activity at 100 μM Ca^{2+}, and 1,000 for H2 activity at 100 μM Ca^{2+}. The solid lines illustrate the fit to simulation of data using the rate constants given in Table 4 (channel 1) for L activity and the rate constants given in Results for H1 and H2 activity.

mode decreases and in H1 mode increases with increasing $[Ca^{2+}]$. For example, for one channel the rate constant for the L→H1 transition was evaluated to be 0.002 μM^{-1} s^{-1}, and the rate constant for H1→L transition was evaluated to be 0.25 s^{-1}.

DISCUSSION

In agreement with the work of Zahradníková and Zahradník (1995) on native canine cardiac RyRs, we observed that native sheep cardiac RyR channels exhibit modal gating. We also found that the gating of the purified channel was

characterized by essentially identical modal behavior as the native channel. Our results indicate that the Ca^{2+}-activated channel may gate in more than the two active modes, H and L, described previously (Zahradníková and Zahradník, 1995). We observed the channels to gate in three active modes, L, H1, and H2, although H2 was not common until the $[Ca^{2+}]$ was raised to ~50 μM or higher. Zahradníková and Zahradník (1995) may not have observed this mode because their analysis of modal gating was performed only for data obtained at 15 μM Ca^{2+}, a $[Ca^{2+}]$ at which Po was low and at which the percentage time the channels gate in H2 mode would be extremely low.

The open lifetime distributions within L mode were independent of the cytosolic $[Ca^{2+}]$. Neither the time constants nor the areas were altered by increasing $[Ca^{2+}]$, indicating that Ca^{2+} does not bind to the open states in L mode. With increasing $[Ca^{2+}]$, the mean closed lifetimes decreased, demonstrating that the mechanism for the increase in Po with Ca^{2+} within L mode is due solely to an increase in the frequency of channel opening. The mean open lifetime in H1 and especially H2 modes were higher than in L mode. The longest open exponential components are associated with H2 mode gating, and Ca^{2+} may bind with open states in H2 mode as we observe a decrease of two open time constants with an increase of $[Ca^{2+}]$. Although the open and closed lifetime distributions were markedly different for different modes, they were very similar for native and purified channels for the same mode of activity.

We have previously only been able to resolve three significant exponential components to the open lifetime distribution even at the higher $[Ca^{2+}]$, although we observed a trend toward an increase in mean open lifetime and in all three open lifetime time constants (Sitsapesan and Williams, 1994b). By separating the events into H and L activity it becomes clear that the trend toward the increased mean open lifetimes as $[Ca^{2+}]$ is increased results from the increase in H activity occurrence relative to L activity occurrence. H1 and H2 modes are characterized by longer open states and a larger contribution of longer open states to the open lifetime distribution than occurs in L activity.

We estimated the single-channel kinetic parameters and proposed different kinetic schemes for the description of three gating types of activity. For L activity, although there were some differences in the rate constants from channel to channel, the maximum likelihood algorithm for the subsets of data from all analyzed channels converged to the same kinetic schemes. The schemes for all the channels had the same ranking using the Schwarz criterion and exhibited similar trends in the relative magnitudes of the rate constants. Scheme 1 excellently predicted the lifetime distributions at different $[Ca^{2+}]$ and the relationships between the mean durations of adjacent intervals. Scheme 1 is similar to the empirical scheme proposed earlier by Sitsapesan and

Williams (1994b) to describe the gating of the sheep cardiac RyR in response to activation by cytosolic Ca^{2+}.

We observed a higher probability of the channel gating with H activity and higher Po within L mode at positive potentials than at negative potentials. The extraction of rate constants at $+40$ and -40 mV indicates that the observed voltage dependence of RyR channel gating may be the result of an increase in RyR channel Ca^{2+} sensitivity at positive potentials.

Our prediction of the schemes for H1, and especially H2, modes is less certain than that for L mode because of the relatively smaller amounts of data for H activity in comparison with L activity and because analyzable quantities of data could be obtained only at two $[Ca^{2+}]$. Although the proposed kinetic scheme gives a good prediction of experimental lifetime distributions (including conditional lifetime distributions) we do not exclude the possibility that more likely models exist.

Information about the Ca^{2+} dependence of the different modes and of the Ca^{2+} dependence of the relative occurrence of the different modes is important when trying to understand how the kinetic schemes for H and L modes of channel activity may be connected. Our observations concerning modal gating do not agree with previous explanations of the gating mechanisms involved in the adaptation observed when cytosolic $[Ca^{2+}]$ is rapidly raised using flash photolysis of a caged Ca^{2+} compound. It has been suggested that the adaptation is due to the transition of the channel from H mode to an equilibrium mixture of modes (Zahradníková and Zahradník, 1995; Armisén et al., 1996). In the model described by Zahradníková and Zahradník (1996), the Po within L mode was Ca^{2+} independent and increasing $[Ca^{2+}]$ decreased the probability of H mode occurrence and increased the probability of I and L mode occurrence. The authors suggested that their model of modal gating behavior can arise because at the onset of the elevation in $[Ca^{2+}]$, Ca^{2+} can bind only in H mode, which is directly accessible from the resting state (Po increases because of the increase in Po within H mode with increasing $[Ca^{2+}]$). If this were the case, the mean time of the Ca^{2+}-binding step would decrease with increasing $[Ca^{2+}]$ and the probability of H mode occurrence would decrease only if the transition from L to H mode was not strongly Ca^{2+} dependent. Our experimental observations, however, demonstrate the involvement of multiple Ca^{2+}-binding sites and that increasing cytosolic $[Ca^{2+}]$ causes an increase in Po within L mode and an increase in the relative occurrence of H modes.

An additional observation also confirms that a model of adaptation is inconsistent with our experimental data. According to the model of adaptation, RyR channels are predominantly in H mode at low $[Ca^{2+}]$. However, inspection of our data at 10 μM Ca^{2+} demonstrate that the open lifetime distribution for the total recordings is close to that for L but not H1 mode. Therefore, the channels

cannot be predominantly in H mode at low $[Ca^{2+}]$. Clearly, our data cannot be reconciled with the gating models described by Zahradníková and Zahradník (1996, 1999). We would predict that the increasing relative occurrence of H modes that we observe in response to an increase in cytosolic $[Ca^{2+}]$ would occur if, for example, the state C1 in the L activity kinetic scheme is in the resting state and the state C4 in the L activity scheme is directly connected to state C1 in the H1 activity scheme. We have drawn this conclusion from the analysis of theoretical steady-state probabilities of the states in L and H1 activity for the gating schemes connected by slow transitions between different possible states. Our kinetic models for the gating of the sheep cardiac RyR channel, based on experimental steady-state recordings, predict, therefore, that adaptation would not occur in response to a rapid step change in $[Ca^{2+}]$. These results are in line with our previous observations that rapid step changes in cytosolic $[Ca^{2+}]$ produce RyR channel activation with no evidence of adaptation although inactivation mechanisms are clearly present under certain conditions (Sitsapesan et al., 1995). Indeed, the results confirm our opinion that the adaptation observed in response to flash photolysis of caged Ca^{2+}, and the inactivation observed in response to a step change in $[Ca^{2+}]$, described by several groups, are quite distinct mechanisms (Sitsapesan et al., 1995; Laver and Curtis, 1996; Schiefer et al., 1995; Lamb and Laver, 1998).

It has previously been reported that purified RyR channels do not exhibit the decaying phase of activity after flash photolysis (Velez et al., 1995) and that this can be explained by the lack of a regulatory protein. If adaptation is due to the transition of the channel from H mode to an equilibrium mixture of modes (Zahradníková and Zahradník, 1995; Armisén et al., 1996) then it would be expected that the modal gating behavior of purified channels would exhibit distinct differences to that of the native channel, based on the assumption that the putative regulatory protein is removed during purification. However, our observation that purified channels exhibit similar modal gating to native channels, with no differences in intra- or inter-modal behavior, indicates that the absence of adaptation in purified channels is not a result of a lack of modal shifts.

As both our analysis of modal gating and the experimental observations of the gating of channels activated by rapid changes in $[Ca^{2+}]$ from our own and other laboratories (Sitsapesan et al., 1995; Laver and Curtis, 1996; Schiefer et al., 1995) indicate that neither native nor purified channels may adapt to a Ca^{2+} stimulus, it is clear that other inactivation mechanisms must be considered as possible mechanisms for the cessation of SR Ca^{2+} release during excitation-contraction coupling in cardiac cells. There are many possible inactivation mechanisms that could control the closure of cardiac RyR channels, and some of these have been discussed in detail (Lamb

and Laver, 1998). Laver and Lamb (1998) found a correlation between channel inactivation and long-lived open states. In our model, however, the long closed state was not connected with the longest open state. This is perhaps not surprising because voltage-dependent inactivation of the type observed by Laver and Lamb (1998) and Sitsapesan and Williams (1995) was not observed in the experimental data set used here as it is usually observed in the presence of a second activating ligand (for example, ATP or caffeine).

In summary, using a quick and powerful maximum likelihood algorithm with a missed-events correction (Qin et al., 1996, 1997) for estimating single-channel kinetic parameters from idealized data recordings we have selected distinct kinetic schemes describing the gating for low and high RyR channel activity. We find that both native and purified channels reconstituted into planar phospholipid bilayers exhibit modal gating when activated by cytosolic Ca^{2+}. Such spontaneous shifts in channel activity are likely to contribute significantly to the variability, in response to changes in Ca^{2+}, that is observed by many workers (Sitsapesan and Williams, 1994b; Percival et al., 1994; Zahradníková and Zahradník, 1995; Copello et al., 1997) but would not, in the absence of some additional mechanism, be sufficient to lead to adaptation to a maintained Ca^{2+} stimulus. We therefore suggest that other mechanisms of RyR inactivation, such as the voltage-dependent type of inactivation reported previously (Sitsapesan and Williams, 1995; Laver and Lamb; 1998), are likely to be responsible for inactivation of RyR channels during excitation-contraction coupling in cardiac cells. Our models of RyR gating can be used as the basis for further experimentation and as tools for unraveling the mechanisms underlying activation and inactivation of the cardiac RyR.

REFERENCES

Armisén, R., J. Sierralta, P. Vélez, D. Naranjo, and B. A. Suárez-Isla. 1996. Modal gating in neuronal and skeletal muscle ryanodine-sensitive Ca^{2+} release channels. *Am. J. Physiol.* 271:C144–C153.

Ashley, R. H., and A. J. Williams. 1990. Divalent cation activation and inhibition of single calcium release channels from sheep cardiac sarcoplasmic reticulum. *J. Gen. Physiol.* 95:981–1005.

Cheng, H., M. Fill, H. Valdivia, and W. J. Lederer. 1995. Models of Ca^{2+} release channel adaptation. *Science.* 267:2009–2010.

Chu, A., M. Fill, E. Stefani, and M. L. Entman. 1993. Cytoplasmic Ca^{2+} does not inhibit the cardiac muscle sarcoplasmic reticulum ryanodine receptor Ca^{2+} channel, although Ca^{2+}-induced Ca^{2+} inactivation of Ca^{2+} release is observed in native vesicles. *J. Membr. Biol.* 135:49–59.

Colquhoun, D., and A. G. Hawkes. 1995. The principles of the stochastic interpretation of ion-channel mechanisms. *In* Single Channel Recording. B. Sakmann and E. Neher, editors. Plenum Press, New York. 397–479.

Copello, J. A., S. Barg, H. Onoue, and S. Fleischer. 1997. Heterogeneity of Ca^{2+} gating of skeletal muscle and cardiac ryanodine receptors. *Biophys. J.* 73:141–156.

Gibb, A. J., and D. Colquhoun. 1992. Activation of NMDA receptors by L-glutamate in cells dissociated from adult rat hippocampus. *J. Physiol.* 456:143–179.

Györke, S. 1999. Ca^{2+} spark termination: inactivation and adaptation may be manifestations of the same mechanism. *J. Gen. Physiol.* 114:163–166.

Horn, R., and K. Lange. 1983. Estimating kinetic constants from single channel data. *Biophys. J.* 43:207–223.

Horn, R., and C. A. Vandenberg. 1984. Statistical properties of single sodium channels. *J. Gen. Physiol.* 84:505–534.

Keizer, J., and L. Levine. 1996. Ryanodine receptor adaptation and Ca^{2+}-induced Ca^{2+} release-dependent Ca^{2+} oscillations. *Biophys. J.* 71:3477–3487.

Lamb, G. D., and D. R. Laver. 1998. Adaptation, inactivation and inhibition in ryanodine receptors. *In* The Structure and Function of Ryanodine Receptors. R. Sitsapesan and A.J. Williams, editors. Imperial College Press, London. 269–290.

Laver, D. R., and B. A. Curtis. 1996. Response of ryanodine receptor channels to Ca^{2+} steps produced by rapid solution. *Biophys. J.* 71:732–741.

Laver, D. R., and G. D. Lamb. 1998. Inactivation of Ca^{2+} release channels (ryanodine receptors RyR1 and RyR2) with rapid steps in $[Ca^{2+}]$ and voltage. *Biophys. J.* 74:2352–2364.

Laver, D. R., L. D. Roden, G. P. Ahern, K. R. Eager, P. R. Junankar, and A. F. Dulhunty. 1995. Cytoplasmic Ca^{2+} inhibits the ryanodine receptor from cardiac muscle. *J. Membr. Biol.* 147:7–22.

McManus, O. B., A. L. Blatz, and K. L. Magleby. 1985. Inverse relationship of the durations of adjacent open and shut intervals for chloride and potassium channels. *Nature.* 317:625–627.

McManus, O. B., and K. L. Magleby. 1989. Kinetic time constants independent of previous single-channel activity suggest Markov gating for a large conductance Ca-activated K channel. *J. Gen. Physiol.* 94:1037–1070.

Nowycky, M. C., A. P. Fox, and R. W. Tsien. 1985. Long-opening mode of gating of neuronal calcium channels and its promotion by the dihydropyridine calcium agonist Bay K 8644. *Proc. Natl. Acad. Sci. U.S.A.* 82:2178–2182.

Percival, A. L., A. J. Williams, J. L. Kenyon, M. M. Grinsell, J. A. Airey, and J. L. Sutko. 1994. Chicken skeletal muscle ryanodine receptor isoforms: ion channel properties. *Biophys. J.* 67:1834–1850.

Qin, F., A. Auerbach, and F. Sachs. 1996. Estimating single-channel kinetic parameters from idealized patch-clamp data containing missed events. *Biophys. J.* 70:264–280.

Qin, F., A. Auerbach, and F. Sachs. 1997. Maximum likelihood estimation of aggregated Markov processes. *Proc. R. Soc. Lond.* 264:375–383.

Rao, C. R. 1973. Linear Statistical Inference and Its Applications. John Wiley and Sons, New York.

Rousseau, E., and G. Meissner. 1989. Single cardiac sarcoplasmic reticulum Ca^{2+}-release channel: activation by caffeine. *Am. J. Physiol.* 256:H328–H333.

Sachs, F., F. Qin, and P. Palade. 1995. Models of Ca^{2+} release channel adaptation. *Science.* 267:2010–2011.

Schiefer, A., G. Meissner, and G. Isenberg. 1995. Ca^{2+} activation and Ca^{2+} inactivation of canine reconstituted cardiac sarcoplasmic reticulum Ca^{2+}-release channels. *J. Physiol.* 489:337–348.

Schwarz, G. 1978. Estimating the dimension of a model. *Ann. Stat.* 6:461–464.

Sitsapesan, R., R. A. P. Montgomery, and A. J. Williams. 1995. New insights into the gating mechanisms of cardiac ryanodine receptors revealed by rapid changes in ligand concentration. *Circ. Res.* 77:765–772.

Sitsapesan, R., and A. J. Williams. 1994a. Regulation of the gating of the sheep cardiac sarcoplasmic reticulum Ca^{2+}-release channel by luminal Ca^{2+}. *J. Membr. Biol.* 137:215–226.

Sitsapesan, R., and A. J. Williams. 1994b. Gating of the native and purified cardiac SR Ca^{2+}-release channel with monovalent cations as permeant species. *Biophys. J.* 67:1484–1494.

Stern, M. D., L. S. Song, H. Cheng, J. S. K. Sham, H. T. Yang, K. R. Boheler, and E. Ríos. 1999. Local control models of cardiac excitation-contraction coupling: a possible role for allosteric interactions between ryanodine receptors. *J. Gen. Physiol.* 113:469–489.

Tang, Y., and H. G. Othmer. 1994. A model of calcium dynamics in cardiac myocytes based on the kinetics of ryanodine-sensitive calcium channels. *Biophys. J.* 67:2223–2235.

Velez, P., X. Li, R. Tsushima, A. Cortes-Gutierrez, A. Wasserstrom, and M. Fill. 1995. Adaptation of single cardiac ryanodine receptor channels may involve a closely associated regulatory protein. *Biophys. J.* 68: A375.

Villalba-Galea, C. A., B. A. Suarez-Isla, M. Fill, and A. L. Escobar. 1998. Kinetic model for ryanodine receptor adaptation. *Biophys. J.* 74:A58. (Abstr.)

Zahradníková, A., and I. Zahradník. 1995. Description of modal gating of the cardiac calcium release channel in planar lipid membranes. *Biophys. J.* 69:1780–1788.

Zahradníková, A., and I. Zahradník. 1996. A minimal gating model for the cardiac calcium release channel. *Biophys. J.* 71:2996–3012.

Zahradníková, A., I. Zahradník, I. Györke, and S. Györke. 1999. Rapid activation of the cardiac ryanodine receptor by submillisecond calcium stimuli. *J. Gen. Physiol.* 114:787–798.